




# Wildland Fire Spread Modeling Using Convolutional Neural Networks

Jonathan L. Hodges\* , and Brian Y. Lattimer, Jensen Hughes, 2020 Kraft Drive, Suite 3020, Blacksburg, VA 24060, USA

**Received:** 11 November 2018/**Accepted:** 19 March 2019

**Abstract.** The computational cost of predicting wildland fire spread across large, diverse landscapes is significant using current models, which limits the ability to use simulations to develop mitigation strategies or perform forecasting. This paper presents a machine learning approach to estimate the time-resolved spatial evolution of a wildland fire front using a deep convolutional inverse graphics network (DCIGN). The DCIGN was trained and tested for wildland fire spread across simple homogeneous landscapes as well as heterogeneous landscapes having complex terrain. Data sets for training, validation, and testing were created using computational models. The model for homogeneous landscapes was based on a rate of spread from the model of Rothermel, while heterogeneous spread was modeled using FARSITE. Over 10,000 model predictions were made to determine burn maps in 6 h increments up to 24 h after ignition. Overall the predicted burn maps from the DCIGN-based approach agreed with simulation results, with mean precision, sensitivity, F-measure, and Chan–Vese similarity of 0.97, 0.92, 0.93, and 0.93, respectively. Noise in the input parameters was found to not significantly impact the DCIGN-based predictions. The computational cost of the method was found to be significantly better than the computational model for heterogeneous spatial conditions where a reduction in simulation time of  $10^2$ – $10^5$  was observed. In addition, the DCIGN-based approach was shown to be capable of predicting burn maps further in the future by recursively using previous predictions as inputs to the DCIGN. The machine learning DCIGN approach was able to provide fire spread predictions at a computational cost three orders of magnitude less than current models.

**Keywords:** Wildland fire, Machine learning, Neural network, Fire spread, Convolutional neural network, CNN, DCIGN

## 1. Introduction

Wildland fire propagation is a complex process which involves the interactions of many underlying physical phenomena. Simulating the spatial-temporal fire front across diverse landscapes for large fires may take hours to run depending on the size of the fire perimeter. Considering the impact of varying weather conditions

---

\* Correspondence should be addressed to: Jonathan L. Hodges, E-mail: [jhodges@jensenhughes.com](mailto:jhodges@jensenhughes.com)



and different intervention strategies on the fire spread requires multiple simulations that may limit the number of scenarios which can be analyzed during an emergency. A new wildland fire spread model is needed that is capable of predicting the two-dimensional spatial-temporal fire front for wildland fires spreading over diverse landscapes, fuel types, and weather conditions which provides rapid predictions regardless of fire perimeter size. Existing wildland fire spread models generally fall into three categories: stochastic, phenomenological, and physical. A number of different fire spread model approaches have been proposed with each class of model having different advantages and limitations [1–3].

Stochastic fire spread models are based on statistical analysis of historical wildland fires and prescribed burns. Sullivan examined 14 stochastic models developed between 1990–2013 and found each could be summarized by the functional form chosen to describe the impact of wind speed, zero wind fire spread, and fuel moisture content [3]. The impact of wind on wildland fire spread generally follows a power law where the exponent and pre-factor are related to the fuel type. The impact of fuel moisture content on wildland fire spread is generally modeled as strongly linear or weakly exponential based on the fuel type. These models are capable of providing rapid reasonable estimates of the overall fire risk of the region for which they were derived. However, stochastic models fail when predicting conditions outside the historical data, such as new weather conditions, spatial regions, or different fuel types [4]. In addition, these models generally make no attempt at resolving the spatial-temporal flame front of a wildland fire.

Phenomenological fire spread models are based on conservation of energy, but use experimental measurements to develop functional forms rather than modeling from first principles [1, 3]. The most widely known phenomenological rate of spread model is the model of Rothermel [5, 6] which uses empirical correlations for heat source and sink terms [1]. The baseline rate of spread (with no wind or slope) is based on fuel density, type, and moisture content. The impact of wind and slope is modeled as a multiplier of the baseline rate of spread. Although developed to determine the rate of spread from a single ignition source in a single direction, these models have been expanded to work in two-dimensions using Huygens' principle [7, 8] and the level set method [9, 10]. These models are favored by foresters and firefighters in the field as they are capable of providing rapid estimates of the rate of spread [4]. However, phenomenological models inherit similar issues to stochastic models when predicting conditions outside the historical data used in deriving the empirical models. In addition, expanding the model to two-dimensions to predict the spatial-temporal fire front significantly increases the computational requirements.

Physical fire spread models are based on the fundamental chemistry and physics of combustion, and fire spread [2]. Physical models can be further subdivided into simple and detailed models. Simple physical models such as that of Weber consider only the transport of energy, neglecting calculation of the full flow field for computational reasons [1]. These models are more general than stochastic or phenomenological models and can be close to real-time [4]. Detailed physical models such as Wildland-Urban Interface Fire Dynamics Simulator (WFDS) consider the transport of mass, momentum, and energy in addition to combustion in a multi-phase approach through computational fluid dynamics (CFD) [11]. These models

are favored by researchers interested in the fundamental mechanisms of wildland fire spread as the basis on first principles reduces the impact of user intuition on the results. However, the computational cost to model moderate domains ( $2.25 \text{ km}^2$ ) is significant [11].

Researchers have recently used reduced order modeling to decrease the computational cost of evaluating these models. This type of approach uses mathematical tools such as proper orthogonal decomposition (POD) to project complex non-linear equations to a reduced order space. Lattimer et al. applied a POD–DEIM approach to calculate the temperature front of a one-dimensional wildland fire based on an advection–reaction–diffusion equation [12]. The authors showed a decrease in computational time of  $10^2$ – $10^3$  over directly solving the partial differential equations. The method presented by Lattimer et al. works for fire spread over homogeneous terrain; however, a new formulation of the projected equations is needed to incorporate different fuel loadings and reaction rates in order to predict fire spread over heterogeneous terrain.

Researchers have recently used data assimilation approaches to improve these models. Data assimilation models fuse a forward prediction scheme with real-time observations to improve model predictions over time. One approach uses observations of the fire perimeter to update the model predicted fire perimeter at specific time intervals. Since the fire perimeter is corrected as new observations are obtained, the error in the predicted fire perimeter is low after a correction. However, the inputs to the forward model are not updated between model predictions which can result in the model error growing between assimilated observations. Researchers have addressed this limitation by using the observation data with an inverse modeling approach to update unknown model parameters (such as wind speed, moisture content, or fuel loading) rather than directly updating the fire perimeter. Several researchers have shown the capability of these models to determine optimal model inputs from inverse modeling [10, 13–17]. The accuracy of the inverse modeling approaches depend on the statistics of the invariant parameters not changing and the accuracy of the underlying forward model. The fusion of observations and predictions in both approaches is generally accomplished through the use of a filter. Researchers have used both particle filters [18–21] and ensemble Kalman filters [13–17, 22, 23] to improve model predictions of fire perimeter. The computational time required for data assimilation models depends on the computational time used in the forward model as well as the time required for the optimization of invariant parameters. The accuracy of data assimilation models generally increases as the time since ignition increases and more data is assimilated into the model.

Recently, machine learning has been used to predict physics based problems. Machine learning models use observed knowledge about a problem to make predictions of new inputs, often using artificial neural networks. A key difference between these approaches and the data assimilation based approaches is the forward simulation model is learned from the data, which means predictions of new scenarios do not rely on other models or prior knowledge of the system. At a fundamental level, artificial neural networks are massively parallel systems of equa-

tions. Each equation in the system, or neuron, uses information from other neurons in the network to make a single, new observation. Each neuron has a set of weights (which describe the relative importance of each input to that particular equation) and a bias (which describes the threshold magnitude of all the inputs needed to activate the neuron). Pairs of known input and output data are used during the training process to update these weights and biases for each equation in the system. Several researchers have presented machine learning approaches to estimate the total burned area of a fire based on meteorological data [24–28]. Each of these methods is capable of predicting the total burned area; however, no attempts have been made to estimate the time-resolved spatial evolution of a wildland fire front. A machine learning approach to predict the spatially-resolved final burned region of a wildland fire was presented by McCormick. The model used an artificial neural network to classify the the center pixel of a  $3 \times 3$  neighborhood of pixels as burned or unburned [29, 30]. The initial results are promising; however, the model relies on the assumed ellipsoidal growth profile in the direction of wind [7] and only predicts the final burned region but not the time-resolved evolution of spread. The number of neurons needed to make new predictions increase with the complexity of the system and the number of outputs to be predicted. Historically this has limited the capability of artificial neural networks to predict the spatial-temporal development of the fire front.

Often in wildland fire spread modeling, there is a need to predict the spatially resolved fire front. Convolutional neural networks (CNNs) were first presented by LeCun in 1989 [31] and recently popularized by Krizhevsky in the 2012 ImageNet competition [32]. The fundamental principle of a CNN is the idea that the data has a meaningful grid-like relationship [33]. Since the network assumes spatial dependence, less connections need to be made to inputs which are far from each other. This allows a CNN to contain much fewer connections and parameters than a similarly sized standard feed forward network with minimal loss in optimal performance for appropriate problems. In addition, this makes it possible to use deeper and more broad hidden layers without increasing computational requirements beyond what is feasible on current technology [32].

The fundamental principle which makes convolutional neural networks (CNNs) versatile is the capability to learn how to represent complex shapes as combinations of high level feature maps. In a CNN neurons are arranged into a set of kernels (or filters) which are passed over spatially resolved data (such as images). The output from the CNN is a new image per kernel which corresponds to the response of the image to that filter. These output images can be thought of as a high level feature map corresponding to a specific kernel. Some example kernels may include spatial gradients, gradients between different input fields, and overall magnitudes of inputs. Krizhevsky showed many of the features learned by the CNN in the ImageNet competition described the inter-relationship of the 3 color channels [32]. As an analogy to image classification, data such as elevation, moisture content, and wind speed can be treated as channels in an image. Given enough data, a feature based neural network will be able to learn relationships between these physical parameters which can then be used to predict a future burn map.

Researchers have shown a combination of convolutional and transpose convolutional layers in a network can be used to generate new images [34–38]. This type of network was called a deep convolutional inverse graphic network (DCIGN) by Kulkarni et al. [34]. This type of network generally has three stages. In the first stage convolutional layers are applied to the input data to develop a high-dimensional feature representation of the inputs. The feature response images are then classified using fully-connected layers (this stage can be thought of as a global optimization step). The output of the fully-connected layers is then re-combined into a single new output image through transpose convolutional layers. Kulkarni et al. used this type of approach to generate new images of objects and faces at different viewing angles and lighting than the input. Chen et al. extended the approach to generate new images of faces with changed emotions, changed hairstyle, and the addition/removal of glasses to good effect [35]. Researchers using generative adversarial networks (GANs) have generally used a similar architecture for the generator network architectures [36–38]. Researchers have shown these networks have the capability to learn complex image translation tasks. Zhu et al. presented an unpaired image to image translation approach which was capable of tasks such as replacing zebras with horses and converting photographs into art styles of famous artists such as Monet and Van Gogh [37].

The objective of this study was to develop a machine learning wildland fire spread model to predict the time-resolved spatial evolution of a wildland fire front inspired by advancements in the image processing field. The approach was trained and tested for wildland fire spread across simple homogeneous landscapes as well as heterogeneous landscapes having complex terrain using data generated from computational models. The paper is organized as follows. Section 2.1 describes the computational model used to generate data in this work. Section 2.2 describes the neural network architecture used in this work. Section 2.3 describes the metrics used to measure the performance of the model. Section 2.4 describes the post-processing of the network predictions. Section 3 presents results of the neural network predictions on independent testing data. Section 4 discusses the results, examines the sensitivity of the network predictions to input parameters, and discusses the capability to predict further into the future.

## 2. Methods

A schematic showing a high level view of the solution algorithm is shown in Fig. 1. Each primary driver of wildland fire spread is included as a channel in an image which is input to the DCIGN. The DCIGN then uses its prior training to predict a new image with two channels corresponding to the probability a pixel has burned or not burned in the future. The two probability masks are then post-processed to output a single future burn map. The temporal resolution of 6 h and spatial resolution of one pixel/km physically correspond to available global satellite measurements. The following subsections describe the simulation conditions, network architecture, post-processing, and performance metrics used in this work.

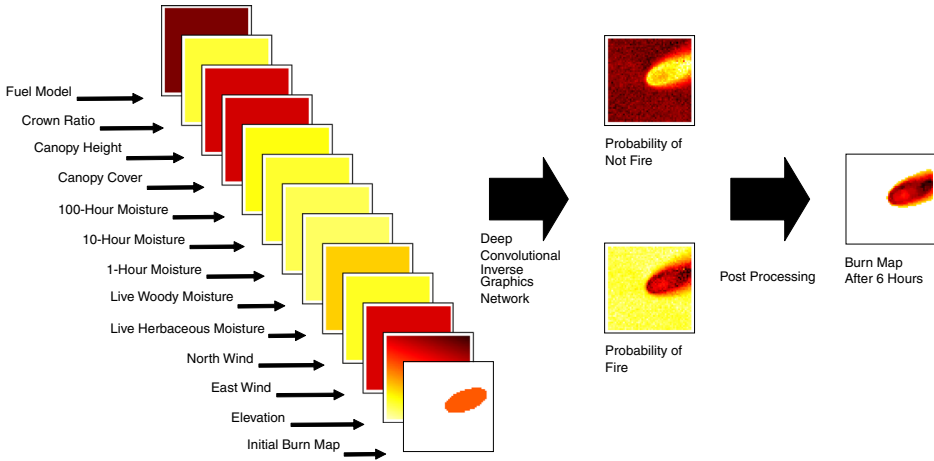


**Figure 1. Schematic of solution algorithm. The left set of images show the different channels used as inputs to the neural network. The values for each data channel are colorized based on the values shown in Tables 1 and 2.**

### 2.1. Wildland Fire Prediction

Data for this study was generated using the surface rate of spread model presented by Rothermel/Albini [5, 6, 39]. In the Rothermel/Albini phenomenological fire spread model, the peak surface fire spread rate,  $V_{s,peak}$  is calculated using the equation

$$V_{s,peak} = \frac{Q''\zeta}{\rho\epsilon Q_{ig}}(1 + \phi_s + \phi_w) \quad (1)$$

where  $Q''$  is the heat release rate per unit area,  $\rho$  is the fuel density,  $Q_{ig}$  is the heat of pre-ignition,  $\zeta$  is the propagating flux ratio (percentage of heat released which pre-ignites fuel),  $\epsilon$  is the effective heating number (percentage of fuel which is involved in ignition),  $\phi_w$  is the wind coefficient, and  $\phi_s$  is the slope coefficient.

Various researchers have developed empirical relationships for the different parameters in Eq. 1. A commonly used approach in the literature is to specify  $Q''$ ,  $\rho$ ,  $\zeta$ ,  $\epsilon$  based on classifying the primary fuel in a region into a fuel model. A total of 53 fuel models were considered in this work including 13 developed by Rothermel/Albini [5, 39], and 40 developed by Scott [6]. Rothermel presented an empirical relationship for  $Q_{ig}$  based on the fuel model and moisture content, and Scott extended the relationship to handle dynamic fuel models. Rothermel presented empirical relationships for  $\phi_w$  and  $\phi_s$  based on fuel model, midflame wind speed, and slope. Andrews presented an algorithm to adjust typical atmospheric wind measurements (10 m or 20 ft) to midflame wind speed based on three additional parameters describing the upper story vegetation (canopy cover, canopy height, and crown ratio) [40]. Researchers have shown wildland fires grow in a generally

**Table 1**  
**Limits of Each Parameter in Study**

Parameter	Unit	Min	Max
Aspect	Degrees	0.0	360
Fuel model	Index	0.0	53
Slope	Fraction	0.0	1.0
1-h moisture	Percent	1.0	40
10-h moisture	Percent	1.0	40
100-h moisture	Percent	1.0	40
Live herbaceous moisture	Percent	30	100
Live woody moisture	Percent	30	100
Canopy cover	Percent	0.0	1.0
Canopy height	Meters	0.3	6.1
Crown ratio	Fraction	0.1	1.0
Wind direction	Degrees	0.0	360
Wind velocity	Kilometers per hour	0.0	48.3

ellipsoidal shape for homogeneous spatial conditions based on  $V_{s,peak}$  and wind speed [7, 41, 42]. The primary drivers in the fire spread model were identified as landscape (slope, aspect, and fuel model type), moisture content (1-h, 10-h, 100-h, live woody, and live herbaceous), canopy type (height, ratio, and percent coverage), and 10 m wind (intensity and direction). The allowable bounds used for each parameter in this work are shown in Table 1. The fuel model types were assigned indexes based on the peak rate of spread under the same spread conditions (low moisture, 10 mph wind up a 0.5 slope). Since slope and aspect can be summarized as a two-dimensional difference in elevation, a single channel for elevation was used instead of two channels for slope and aspect in the neural network.

The model of Rothermel is designed to predict the rate of spread in the peak direction of spread. Predictions in two-dimensions using this model generally rely on the empirical observation that wildland fires generally grow in an ellipsoidal shape for homogeneous spatial conditions based on  $V_{s,peak}$  and wind speed [7, 41, 42]. Using this type of approach, the two-dimensional propagation of the fire from a discrete point is predicted by calculating the heading fire spread velocity and estimating the eccentricity of the ellipse. This corresponds to predicting the two-dimensional spread of a wildland fire over homogeneous landscape and vegetation.

The heading spread rate, or rate of spread in the peak spread direction, is calculated using Eq. 1. The heading spread direction is calculated using the equation

$$\theta = atan(V_y, V_x)$$

(2)

where  $\theta$  is the peak spread direction relative to the slope,  $V_y$  is the  $y$  component of the vector combination of wind spread rate,  $V_w$ , and slope spread rate,  $V_s$ , and  $V_x$  is the  $x$  component of the vector combination of  $V_w$  and  $V_s$ . The slope spread rate is calculated using Eq. 1 with  $\phi_w$  equal to zero. Similarly, the wind spread rate is calculated using Eq. 1 with  $\phi_s$  equal to zero [43].



The backing spread rate, or rate of spread in the opposite direction of the heading spread, is calculated from  $\epsilon$  using the equation

$$V_{s,min} = V_{s,peak} \times \frac{(1.0 - \epsilon)}{(1.0 + \epsilon)} \quad (3)$$

where  $V_{s,min}$  is the backing spread rate, and  $\epsilon$  is the eccentricity of the ellipse. The eccentricity of the ellipse is calculated using the equation [43]

$$\epsilon = \frac{\sqrt{r^2 - 1.0}}{r} \quad (4)$$

where  $r$  is the length-to-width ratio. The length-to-width ratio is calculated using the equation

$$r = 1.0 + 0.25U_{eff} \quad (5)$$

where  $U_{eff}$  is the effective wind speed in the heading direction. The effective wind speed is the magnitude of the vector combination of the ambient wind velocity and the buoyant velocity generated by the fire perimeter [44]. The buoyant velocity generated by the fire perimeter is calculated using the equation

$$U_b = \left( \frac{2gQ_c''}{\rho_a c_{p,a} T_a} \right)^{1/3} \quad (6)$$

where  $U_b$  is the buoyant velocity,  $g$  is the acceleration due to gravity,  $Q_c''$  is the convection component of the heat release rate per unit area,  $\rho_a$  is the air density,  $c_{p,a}$  is the air specific heat capacity, and  $T_a$  is the air temperature.

Homogeneous fire spread based on Rothermel rate of spread was simulated using custom software developed in Python to streamline the integration with the DCIGN software. The implementation of Rothermel's model in BehavePlus was used to verify the custom rate of spread and fire front calculation [43]. Each simulation used a randomly selected combination of the parameters shown in Table 1, selected from a uniform distribution. A total of 10,000 unique combinations of the parameters were simulated.

Burn maps were created by rasterizing the fire perimeter and filling the enclosed region. Raster images of the burn map were generated at a resolution of one pixel/km every 6 h for a total of 24 h/homogeneous fire spread simulation. Three cases for use in the DCIGN were generated from each simulation by creating pairs of burn maps 6 h apart. The 0 h to 6 h pair was not considered as a case for the DCIGN as the 0 h burned image always contains no fire. Example burn maps from one simulation are shown in Fig. 2 for the parameter values shown in Table 2.

Fire spread simulations over heterogeneous landscapes and terrain were completed using FARSITE which has a two-dimensional implementation of Rother-



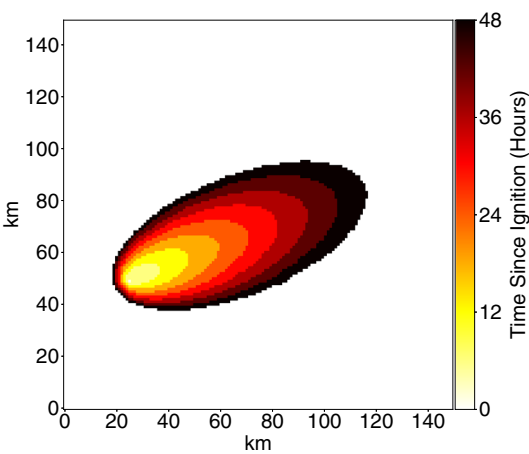


**Figure 2. Example simulated burn maps.**

mel’s rate of spread model [8]. The computational domain for each simulation consisted of a  $50 \times 50$  km domain with a grid resolution of 0.03 km. Each simulation was run for 48 h of fire spread with fire perimeters output every hour of simulation time. Realistic landscape and vegetation maps from the LANDFIRE project were used in this study [45], with 1000 randomly selected regions from the state of California. For each simulation, landscape, vegetation, and non combustible regions were randomly selected from the set of 1000 regions, moisture content and wind speeds were randomized. A total of 2500 FARSITE simulations were used in this study. Burn map pairs were extracted every 6 h, yielding approximately 17,500 scenarios. An example simulated burn map using FARSITE is shown in Fig. 3. The predicted burn maps and spatial inputs were down-sampled to a 1 km spatial grid to match the resolution of the homogeneous fire spread

**Table 2**  
**Parameters for Example Simulation**

Parameter	Unit	Value
Aspect	Degrees	130
Fuel model	Index	FM1 (44)
Slope	Fraction	0.8
1-h moisture	Percent	5.3
10-h moisture	Percent	6.3
100-h Moisture	Percent	7.3
Live herbaceous moisture	Percent	69
Live woody moisture	Percent	49
Canopy cover	Percent	0.7
Canopy height	Meters	4.3
Crown ratio	Fraction	0.2
Wind direction	Degrees	34
Wind velocity	Kilometers per hour	21.7

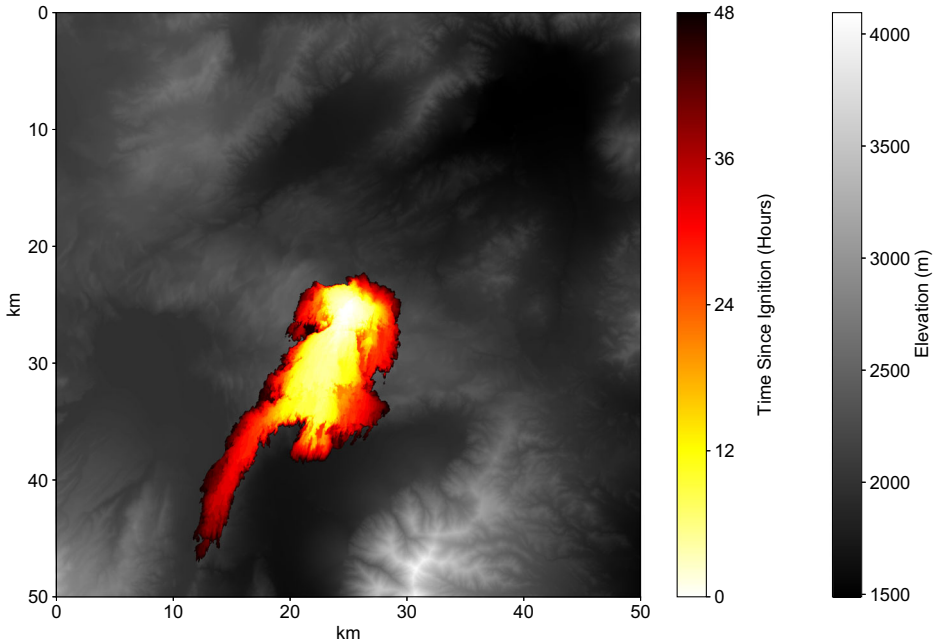


**Figure 3. Example predicted burn map from FARSITE.**

simulations using a median filter. An example set of down-sampled landscape, vegetation, and ambient parameters which were used as inputs and outputs to the DCIGN are shown in Fig. 4.

## 2.2. Network Architecture

The DCIGN architecture used in this work is shown in Fig. 5. The input images were  $50 \times 50$  pixels with 13 image channels corresponding to the image stack shown in Fig. 1. The output image contains  $50 \times 50$  pixels with two image channels corresponding to the probability the burn map has reached a pixel and the probability the burn map has not reached a pixel. A total of six hidden layers are included in the network including two convolutional, two max pooling, one fully connected classification, and one transpose convolutional layers. The number of filters and step size in each convolutional and transpose convolutional layers and number of neurons in fully connected layers were specified to steadily decrease the degrees of freedom from the 32,500 in the input layer ( $50 \times 50 \times 13$  inputs) to the desired degrees of freedom of 5000 in the output layer ( $50 \times 50 \times 2$  probability of fire and not fire).

All layers in the network presented in this work used leaky rectified linear unit (ReLU) activation functions except the fully connected layer which used hyperbolic tangent (TanH) activation functions and the output layer which used a softmax activation function. Researchers have shown deep neural networks learn more quickly and more accurately using leaky or parametric ReLU than logistic

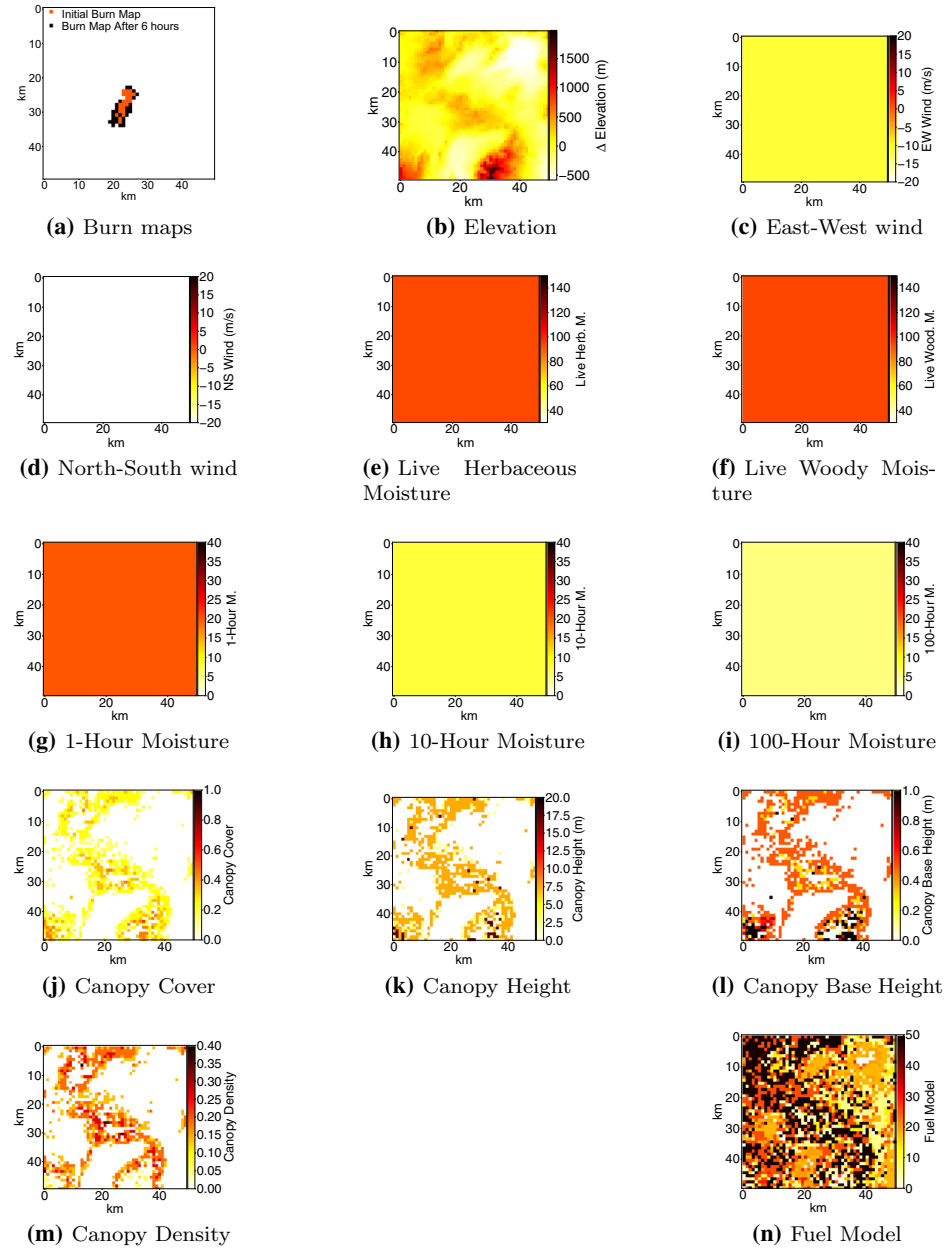


**Figure 4. Example heterogeneous landscape and vegetation.**

or TanH for activation [46, 47]. However, since the activation is unbounded, ReLU is not appropriate for classification layers. Since the intent of the fully connected layer is to classify the feature maps into high level descriptions of the fire and environment, a TanH activation function is appropriate. Since the desired

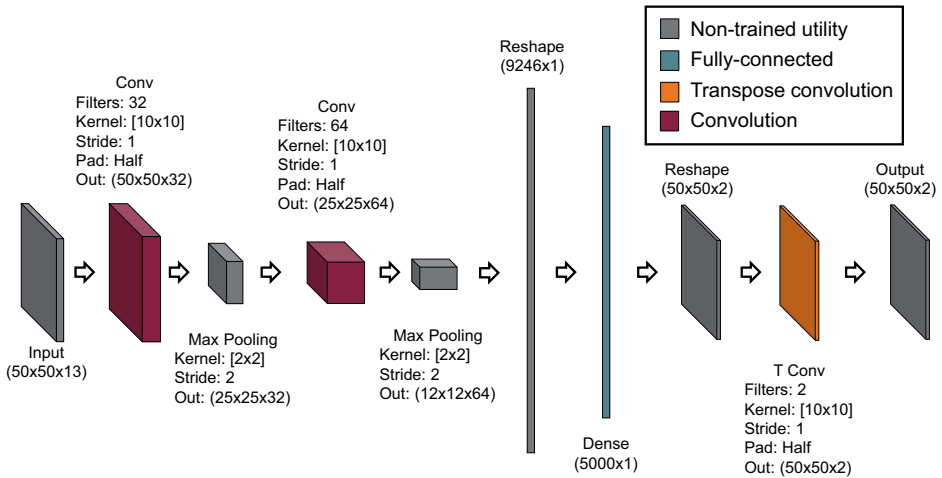


**Figure 5. Deep convolutional inverse graphics network architecture.**

output is a probabilistic estimate of whether or not each pixel would be burned, a soft max activation function is appropriate to scale the activations of the fire and non-fire probability masks.

The network architecture was built using the Python 3 bindings for TensorFlow [48]. The models were trained using stochastic gradient descent with a batch size of 100 samples. All weights and biases were initialized from a uniform distribution between  $-1$  and  $1$ . The learning rate was fixed for all layers throughout training at  $0.0001$ . The cost function used in training the network was sum square error. Over-fitting was reduced by using 50% dropout on the input layer and shuffling the order of the samples during training. The network was trained to predict homogeneous fire spread using 9000 simulations (27,000 pairs of burn maps) for 50,000 cycles using a single NVIDIA Quadro K620. The total time to train the network was 18 h 7 min. The total time to evaluate the network with all 10,000 simulations (30,000 pairs of burn maps) was 38.1 s. The network was trained to predict heterogeneous fire spread using 2215 simulations (15,500 pairs of burn maps) for 250,000 cycles using a single NVIDIA Quadro K620. The total time to train the network was 51 h 33 min. The total time to evaluate the network with all 2500 simulations (17,500 pairs of burn maps) was 185.0 s. The difference in training cycles between the homogeneous and heterogeneous simulations was due to an increase in complexity in the features the network needed to learn. The difference in evaluation time between the homogeneous and heterogeneous simulations was due to different data read-write routines.

### 2.3. Performance Metrics

Researchers have presented several metrics which can be used to analyze the performance of a wildland fire spread model. These metrics are typically either based on statistical classification or shape similarity. Filippi et al. presented an overview

of statistical classification methods such as Sørensen similarity index, Jaccard similarity coefficient, Kappa statistics, and ratio of areas [49]. These metrics generally provide an estimate of the area of intersection and union of the predictions and ground truth; however, do not reveal information regarding the tendency of the model to over-predict or under-predict the ground truth. Metrics such as precision, sensitivity, and F-measure are often used by the image classification community to describe the over/under-prediction of the model. Zhang et al. presented a front shape similarity measure based on Chan–Vese Segmentation (CVS) [50]. The premise of this metric is to apply level set segmentation to a simulated burn map and compare the resultant level set image with the ground truth. The metrics used to quantify the performance of the DCIGN in this study were precision, sensitivity, F-measure, and CVS. For each metric, the range of possible values is zero to one, with a perfect score being one.

The precision,  $P$ , is a measure of commission errors (predicting a fire where there was not fire) and is defined as

$$P = \frac{t_p}{t_p + f_p} \quad (7)$$

where  $t_p$  is the number of correctly identified fire pixels, and  $f_p$  is the number of falsely identified fire pixels. The sensitivity,  $S$ , is a measure of omission errors (predicting no fire where there was a fire) and is defined as

$$S = \frac{t_p}{t_p + f_n} \quad (8)$$

where  $f_n$  is the number of fire pixels which were identified as non-fire pixels. F-measure,  $F$ , is an overall measure of performance defined as the harmonic mean of  $P$  and  $S$ ,

$$F = 2 \cdot \frac{P \cdot S}{P + S}. \quad (9)$$

The CVS is calculated using the formulation presented by Zhang et al. [50], using the equation

$$\text{CVS} = 1 - \int_{\Omega} H_v[y - C_{\max}]^2 + (1 - H_v)[y - C_{\min}]^2 ds \quad (10)$$

where  $y$  is the true burn map,  $H_v$  is the Heaviside function is defined as

$$H_v = \begin{cases} 0 & \text{if } \phi_c < 0 \\ 1 & \text{if } \phi_c > 0 \end{cases} \quad (11)$$

where  $\phi$  is the level-set function as presented by Chan et al. [51], and  $C_{\max}$  and  $C_{\min}$  are scalar coefficients defined by

$$C_{max} = \max(C_0, C_1) \quad (12)$$

and

$$C_{min} = \min(C_0, C_1), \quad (13)$$

respectively. The scalar coefficients are calculated using the equations

$$C_0 = \frac{\int_{\Omega} (1 - H_v) y ds}{\int_{\Omega} (1 - H_v) ds} \quad (14)$$

and

$$C_1 = \frac{\int_{\Omega} H_v y ds}{\int_{\Omega} H_v ds}. \quad (15)$$

The CVS presented in this work is different from that presented by Zhang et al. in two ways. The level-set segmentation method is ill-posed for fires with few total pixels as the level-set function cannot be computed. Thus the CVS presented in this work includes all simulations where the initial fire size is greater than nine pixels. The definition presented by Zhang et al. defines a range of zero to one with a perfect score being zero. For consistency with the statistical measures presented in this work, a 1-CVS term was added to Eq. 10 so that the perfect score is one.

#### 2.4. Post Processing

The output layer of the DCIGN contains two normalized probability masks, one for fire and one for not fire. The normalized probability mask for fire is post-processed to convert the probabilistic estimate of burned or unburned to a single contour. A  $3 \times 3$  median filter is applied to smooth the image. A threshold value on probability of fire is used to determine whether or not each pixel has been burned.

The optimal threshold to use in post-processing was determined by calculating the mean F-measure for DCIGN predictions of the 9000 training simulations (27,000 pairs of burn maps) with thresholds ranging from 0.01 to 0.99. The mean F-measure was found to be mostly independent of the post-processing threshold in the range of 0.2–0.6 as shown in Fig. 6. The maximum mean F-measure of the training data was calculated with a threshold of 0.41. This threshold was fixed and used for post-processing throughout this work. An example neural network prediction before and after post-processing is shown in Fig. 7.

### 3. Results

The robustness of the neural network to predict new fires was examined by considering 1000 simulations (3000 pairs of burn maps) for homogeneous fire spread and 285 simulations (2000 pairs of burn maps) for heterogeneous fire spread

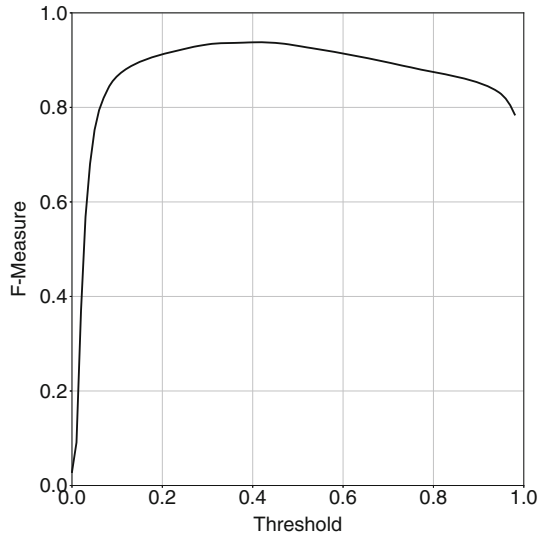


**Figure 6. Mean F-measure of DCIGN predictions of 9000 training simulations (27,000 pairs of burn maps) for different threshold values.**

which were not included when training the network. Sample DCIGN predictions from five of these test cases are compared with simulation predictions in Figs. 8 and 9 for homogeneous and heterogeneous fire spread, respectively. Figures 8a and 9a show the initial and next burn map from the simulation. Figures 8b and 9b show the final burn map predicted by the DCIGN. Figures 8c and 9c highlights pixels which the DCIGN prediction did not match the simulation predictions. Pixels shown as black represent commission errors (false positive of fire), and pixels shown as orange represent omission errors (false negative of fire).

The mean precision, sensitivity, F-measure, and CVS of the 1000 homogeneous fire spread test simulations (3000 burn map pairs) are shown in Table 3. Each metric ranges from zero to one with a perfect score being one. The distribution of F-measure for the 3000 burn map pairs are shown in Fig. 10. Percentiles of each metric are shown in Table 3 to quantify the spread of each score. Here a percentile is defined as

$$X = \frac{1}{N_{total}} \int_{Y_{min}}^1 N(Y) dy \quad (16)$$

where  $X$  is the percentile,  $N(Y)$  is the number of burn maps achieving a specific score,  $N_{total}$  is the total burn maps  $Y_{min}$  is the minimum score. For example, the F-measure of 0.86 for  $X = 80\%$  shown in Table 3 means 80% (2400/3000) of the burn map pairs had an F-measure of 0.86 or higher. Similarly, the mean precision, sensitivity, F-measure, and CVS of the 285 heterogeneous fire spread simulations (2000 burn map pairs) are shown in Table 4. The distribution of F-measure



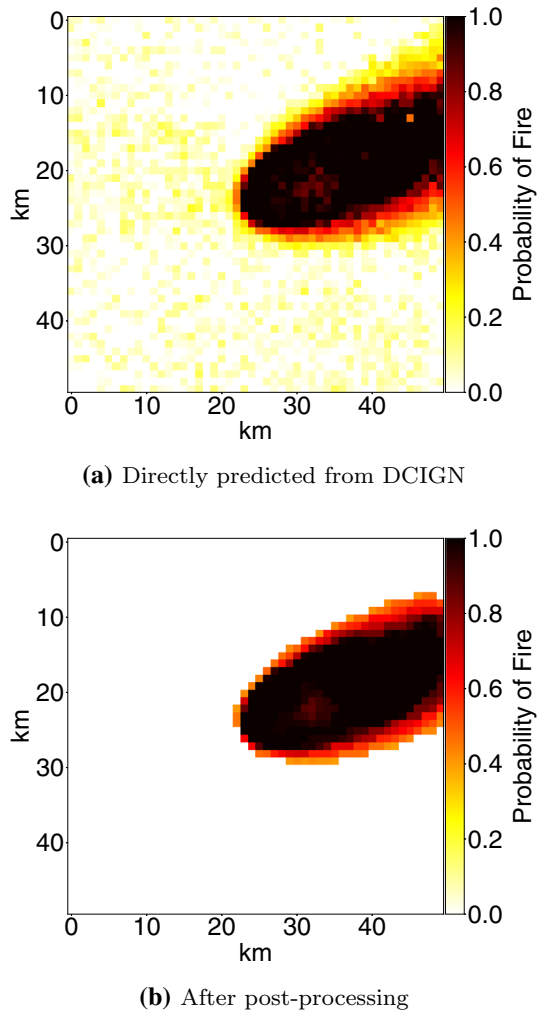


**Figure 7. Example DCIGN prediction of burn map probability.**

for the 2000 burn map pairs are shown in Fig. 11. Figure 11 shows 200 burn map pairs which have a F-measure close to zero, which lowers the performance of the percentiles shown in Table 4. This is discussed in Sect. 4.

## 4. Discussion

The overall shape of the burn maps predicted by the DCIGN are consistent with the simulations for the 1000 homogeneous test simulations and the 285 heterogeneous test simulations examined in this work, as shown in the examples in Figs. 8

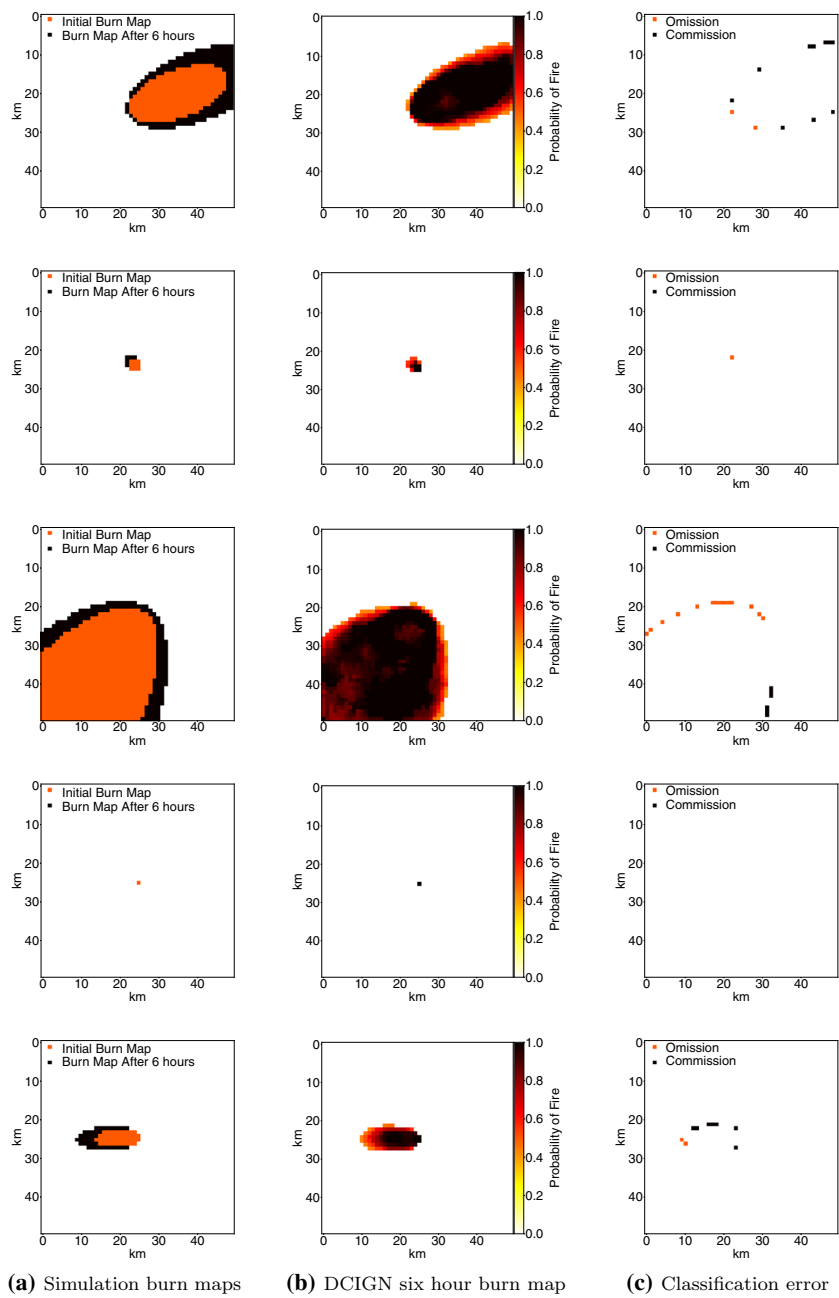


**Figure 8. Example DCIGN prediction results for homogeneous fire spread.**

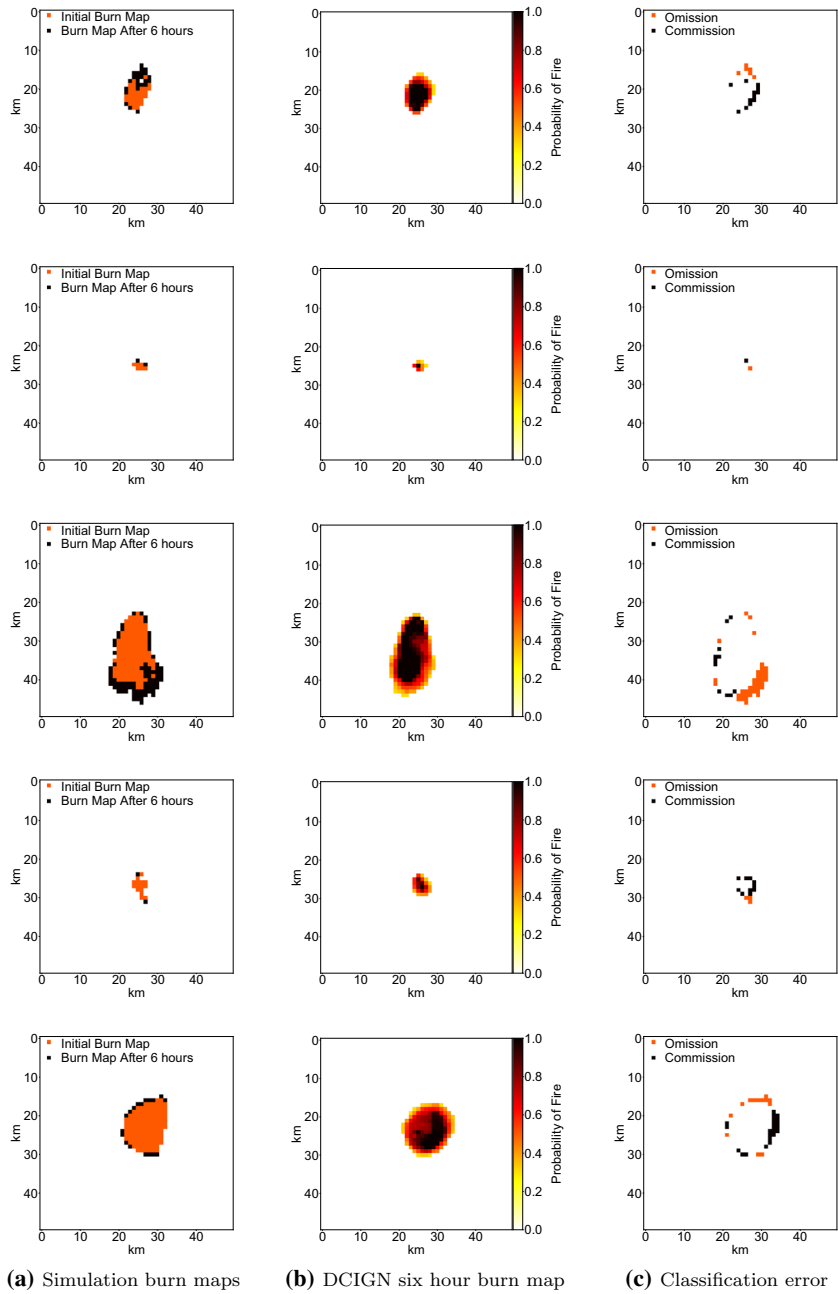


**Figure 9. Example DCIGN prediction results for heterogeneous fire spread.**

**Table 3**  
**Performance Metrics of DCIGN Predictions of Homogeneous Fire Spread Test Cases**

Parameter	Mean	$X = 80\%$	$X = 90\%$	$X = 95\%$
Precision	0.97	0.95	0.85	0.79
Sensitivity	0.92	0.80	0.67	0.59
F-measure	0.93	0.86	0.80	0.73
Chan–Vese similarity	0.93	0.87	0.82	0.77

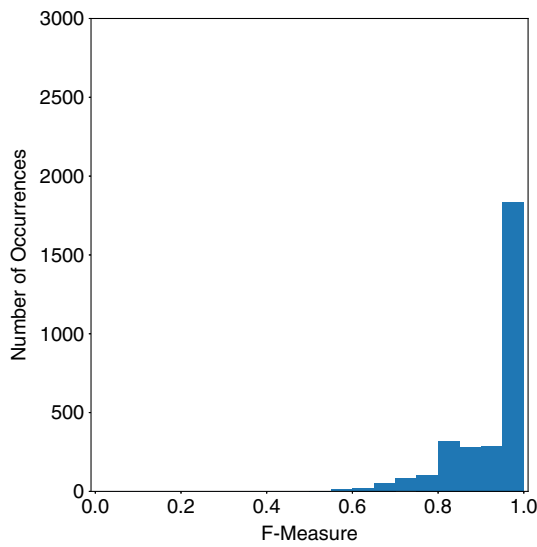


**Figure 10. F-measure distribution of DCIGN predictions of homogeneous fire spread test cases.**

and 9. The burn maps predicted by the DCIGN do not contain non-physical holes or excessive noise. The direction of maximum growth and overall shape is captured well, with a mean CVS of 0.93 and 0.92 for fire spread over homogeneous and heterogeneous terrain, respectively. Figure 8 shows the DCIGN is able to predict the growth of small (1 km<sup>2</sup>, rows 2 and 4), intermediate (10 km<sup>2</sup>, rows 1 and 5), and large (100 km<sup>2</sup> row 3) fires. The first and fifth example in Fig. 9 show regions where the DCIGN predicted fire spread where the simulation did not. One difference in the heterogeneous simulations from the homogeneous simulations was the presence of non-burnable surfaces (typically corresponding to roads, rivers, etc). It was observed that the non-burnable surfaces often corresponded to only one or two pixels in the landscape file. During the down-sampling process these pixels were often removed which resulted in the DCIGN being given no knowledge of the non-burnable surface. These results show the fire spread predic-

**Table 4**  
**Performance Metrics of DCIGN Predictions of Heterogeneous Fire Spread Test Cases**

Parameter	Mean	$X = 80\%$	$X = 90\%$	$X = 95\%$
Precision	0.75	0.64	0.40	0.25
Sensitivity	0.88	0.68	0.25	0.00
F-measure	0.78	0.53	0.21	0.00
Chan–Vese similarity	0.92	0.85	0.77	0.69

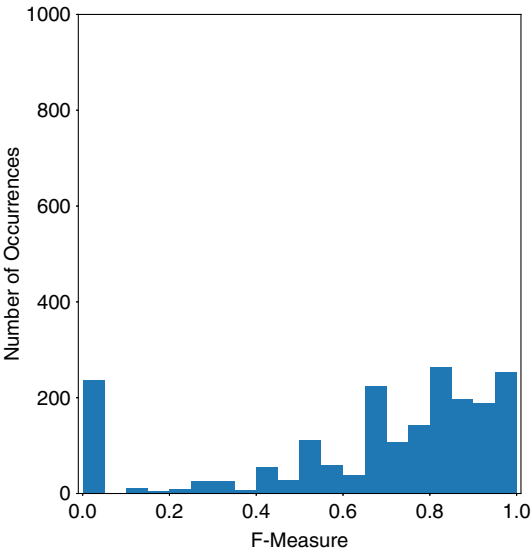


**Figure 11. F-measure distribution of DCIGN predictions of heterogeneous fire spread test cases.**

tions over heterogeneous landscapes should be made at a higher resolution to better capture the impact of non-burnable surfaces.

Across all test cases there was not significant bias observed in over-predicting or under-predicting fires, as is shown by the comparable mean sensitivity and precision shown in Table 3. However, the spread in sensitivity is higher than the spread in precision as is shown by  $X = 80\%$ ,  $X = 90\%$ , and  $X = 95\%$  in Table 3. Examining the histogram of  $F$  for homogeneous fire spread predictions shown in Fig. 10, there is a sharp drop in number of occurrences at  $F < 0.8$ . The initial fire size of 82% of the cases where  $F < 0.8$  was found to be nine pixels or less, as shown in Fig. 12. Combined with the percentiles shown in Table 3, this shows the sensitivity is impacted to a greater extent than precision for small fire sizes. Similar to the DCIGN predictions in the homogeneous case, many scenarios in heterogeneous fire spread with an initial fire with less than 9 pixels resulted in poor

predictions. Figure 13 shows the distribution of F-measure for all cases where the initial fire was greater than 9 pixels in size. The precision, sensitivity, F-measure, and CVS statistics for the heterogeneous test cases with a initial fire greater than 9 pixels in size are shown in Table 5. Since a DCIGN relies on feature recognition, low feature density in the inputs (such as fires less than 9 pixels in size) can lead to a decrease in the accuracy of the model. If smaller fires are of primary interest, this effect could be reduced by increasing the spatial resolution of the model.

The sensitivity of the model to noise in the input parameters was examined by adding noise to the 5 examples shown in Fig. 8 and examining the impact on  $S$ ,  $P$ , and  $F$ . Noise was added by multiplying each input channel by a random value from a log-normal distribution with a mean of 0 and a standard deviation of 1. Note the input and output burn maps were not changed. A total of 3000 iterations for each of the five test cases were predicted by the DCIGN. The zero noise, noise mean, and noise 80% scores for each case for each metric are shown in Table 6. The largest impact was observed in the last test case where the mean and 80% sensitivity dropped from the baseline score by 0.07 and 0.14, respectively. This shows the addition of noise resulted in an increase in the under prediction of the burn map. However, the minimal overall impact on the mean and 80% scores shows the general shape of the predicted burn maps are still in agreement with simulation results.

One of the key benefits of the DCIGN architecture presented in this work is the scalability in heterogeneous spatial conditions. The total time to run 10,000 simulations using the model of Rothermel was 30.6 s compared to the 38.1 s required for the DCIGN. The phenomenological model will likely perform faster whenever evaluating the spread of a fire from a single point in homogeneous conditions.

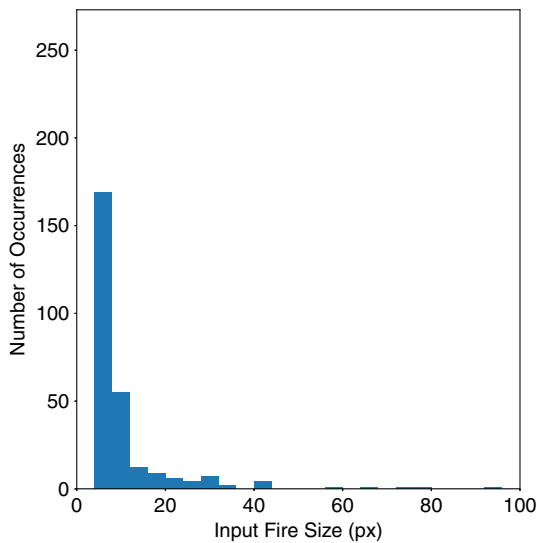


**Figure 12. Distribution of input fire size for all cases where  $F < 0.8$  for homogeneous test cases.**

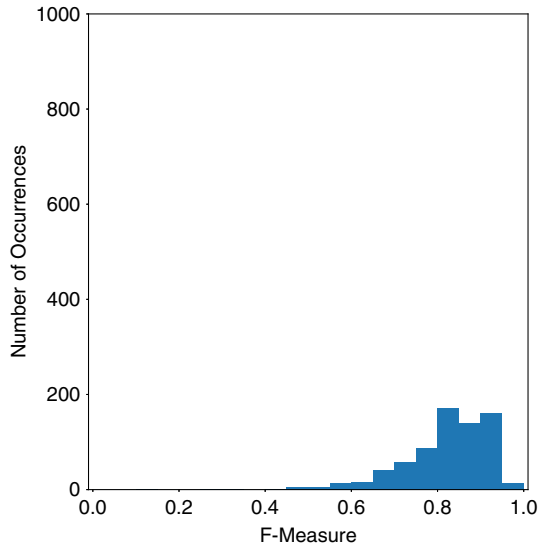


**Figure 13. F-measure distribution of DCIGN predictions of heterogeneous test cases with an initial fire size larger than 9 pixels.**

**Table 5**  
**Performance Metrics of DCIGN Predictions of Heterogeneous Test Cases with Initial Fire Size Larger than 9 Pixels**

Parameter	Mean	$X = 80\%$	$X = 90\%$	$X = 95\%$
Precision	0.89	1.00	0.92	0.80
Sensitivity	0.80	0.94	0.79	0.68
F-measure	0.82	0.91	0.82	0.75
Chan–Vese similarity	0.92	0.85	0.77	0.69

However, when using Huygen’s principle to evaluate Rothermel’s model in heterogeneous spatial conditions, the fire perimeter must be discretized and evaluated for each point along the perimeter. This leads to a significant increase in computational time as the size of the fire increases, as shown in the cumulative probability density of computational time for the 2500 FARSITE simulations used in this study shown in Fig. 14. Approximately 80% of FARSITE simulations took less than hour to run; however, many of the larger fires required 1–6 h of run time. Since the DCIGN is already analyzing all the input channels as two-dimensional image channels, there is no increase in computational cost to add heterogeneous conditions. The total computational time to evaluate all 2500 simulations using the DCIGN method was 185 s, or 0.04 s/simulation. This corresponds to a factor of  $10^2$ – $10^5$  faster than the FARSITE model.



**Table 6**  
**Impact of Noise on Performance Metrics of DCIGN Predictions of Test Cases**

Sensitivity			Precision			F-measure		
Base	Noise	80%	Base	Noise	80%	Base	Noise	80%
0.99	0.98	0.99	0.98	0.98	0.98	0.98	0.98	0.98
0.93	0.91	0.93	1.00	1.00	1.00	0.96	0.94	0.96
0.98	0.97	0.95	0.99	0.99	0.99	0.98	0.98	0.97
1.00	1.00	1.00	1.00	0.93	1.00	1.00	0.95	1.00
0.98	0.91	0.84	0.92	0.90	0.85	0.95	0.90	0.88

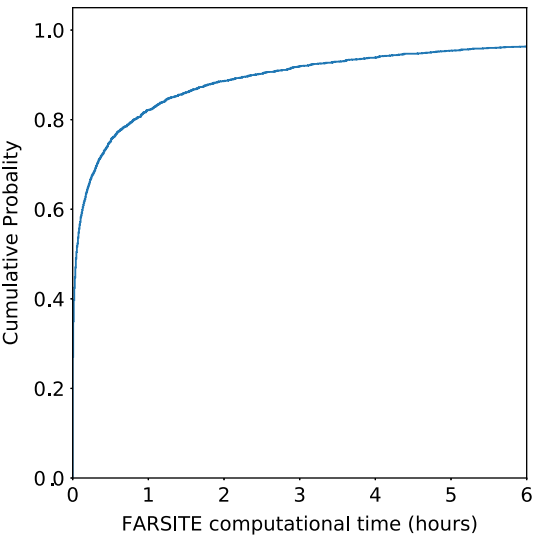


**Figure 14. Cumulative probability of computational time using FARSITE.**

Although the model was trained using a 6 h time interval between the input and output burn maps, it is possible to obtain predictions at points further in the future at 6 h intervals by recursively using the previous prediction as an input to the DCIGN. Figure 15 shows five example cases where this process was used to predict burn maps up to 24 h from ignition based on an input burn map 6 h after ignition. The results for each case show the general direction of spread is captured well, with  $F > 0.8$  in all cases except the fourth case where the input and output fires are small. The sensitivity of the predictions generally increases with time, whereas the precision and CVS generally decreases with time. This shows early in the progression of the fire the model under-predicts the rate of spread, which

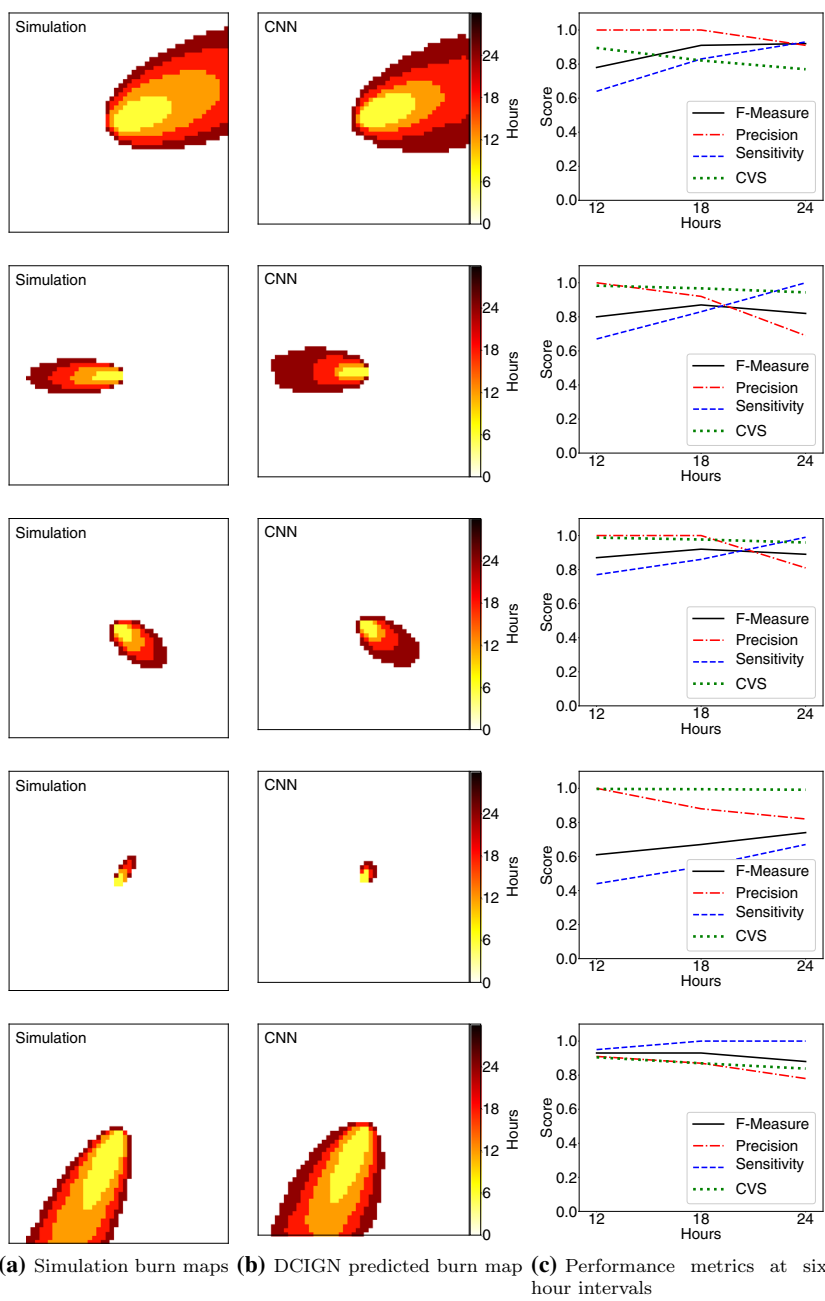


**Figure 15. Example DCIGN prediction of time resolved burn maps.**

highlights the difficulty the DCIGN can have when dealing with low feature density. Later in the progression of the fire, the model begins to over-predict the rate of spread. Since the network was trained on constant rates of spread for each configuration, the over-prediction is likely a result of the network over-correcting for the initial under prediction of rate of spread.

The simulations used in training and testing the DCIGN-based approach used uniform and constant meteorological conditions. Since wind is one of the primary drivers of the evolution of a wildland fire, it is important for a wildland fire spread model to be able to capture the impact of heterogeneous and time-dependent wind conditions. Capturing the impact of heterogeneous wind conditions does not require any adjustments to the approach presented in this work since the underlying mechanism of the DCIGN approach uses spatially resolved features to make future predictions. However, data generated with heterogeneous wind conditions would need to be used in training the model. Adding the impact of time-dependent wind conditions to the model does not require significant changes to the approach. The same recursive approach used to generate the predictions shown in Fig. 15 could be used to incorporate the impact of changing meteorological conditions by adjusting these input channels between predictions. The time-step of 6 h between predictions would likely need to be reduced to capture hourly variation in meteorological conditions.

## 5. Conclusion

This paper presents a machine learning approach to predict the time-resolved spatial evolution of a wildland fire. The DCIGN-based approach was able to predict fire spread over both homogeneous and heterogeneous landscapes with simple and complex terrains. The results presented in this work show feature based neural networks are capable of accurately predicting the propagation of a wildland fire at a fraction of the computational cost of traditional modeling approaches under heterogeneous spatial conditions. One of the advantages of the DCIGN model is the computational requirements are similar for fire spread over homogeneous and heterogeneous terrain. Since a DCIGN relies on feature recognition, low feature density in the inputs (such as fires less than 9 pixels in size) can lead to a decrease in the accuracy of the model. If smaller fires are of primary interest, this effect could be reduced by increasing the spatial resolution of the model. The DCIGN-based approach was able to predict burn maps up to 24 h in the future without a significant decrease in model performance. An advantage of the DCIGN approach over reduced order modeling or data assimilation approaches is it does not rely on any other models at run-time. Although the DCIGN in this work was trained using data generated from a phenomenological model, the model does not have any information whether the data is from a computational fluid dynamics model, phenomenological model, or even experimental measurements. The machine learning DCIGN approach was able to provide fire spread predictions at a computational cost three orders of magnitude less than current models.

## References

1. Weber R (1991) Modelling fire spread through fuel beds. *Prog Energy Combust Sci* 17(1):67
2. Sullivan A (2008) A review of wildland fire spread modelling, 1990-present 1: physical and quasi-physical models. [arXiv:0706.3074v1](https://arxiv.org/abs/0706.3074v1) [physics.geo-ph]
3. Sullivan A (2013) A review of wildland fire spread modelling, 1990-present 2: empirical and quasi-empirical models. [arXiv:0706.4128](https://arxiv.org/abs/0706.4128) [physics.geo-ph]
4. Simeoni A (2015) Wildland fires. In: Hurley MJ, Gottuk DT, Hall JR Jr, Harada K, Kuligowski ED, Puchovsky M, Watts JM Jr, Wieczorek CJ (eds) *SFPE handbook of fire protection engineering*. Springer, pp 3283–3302
5. Rothmel RC et al (1972) A mathematical model for predicting fire spread in wildland fuels. Technical report, USDA Forest Service
6. Scott JH, Burgan RE (2005) Standard fire behavior fuel models: a comprehensive set for use with rothmel's surface fire spread model. Technical report, USDA Forest Service
7. Finney MA (1999) Mechanistic modeling of landscape fire patterns, spatial modeling of forest landscapes: approaches and applications. Cambridge University Press, Cambridge, pp. 186–209
8. Finney MA et al (1998) FARSITE, fire area simulator-model development and evaluation, 3US Department of Agriculture, Forest Service, Rocky Mountain Research Station, Ogden
9. Rehm RG, McDermott RJ (2009) Fire-front propagation using the level set method. US Department of Commerce, National Institute of Standards and Technology, Gaithersburg
10. Lautenberger C (2013) Wildland fire modeling with an eulerian level set method and automated calibration. *Fire Saf J* 62:289
11. Mell W, Jenkins MA, Gould J, Cheney P (2007) A physics-based approach to modelling grassland fires. *Int J Wildland Fire* 16(1):1
12. Lattimer A, Borggaard J, Gugercin S, Luxbacher K, Lattimer B (2016) Computationally efficient wildland fire spread models. In: *Proceedings of the 14th international fire science & engineering conference*, pp 305–315
13. Rochoux MC, Delmotte B, Cuenot B, Ricci S, Trouvé A (2013) Regional-scale simulations of wildland fire spread informed by real-time flame front observations. *Proc Combust Inst* 34(2):2641
14. Rochoux MC, Ricci S, Lucor D, Cuenot B, Trouvé A (2014) Towards predictive data-driven simulations of wildfire spread—part i: reduced-cost ensemble Kalman filter based on a polynomial chaos surrogate model for parameter estimation. *Natural Hazards Earth Syst Sci* 14(11):2951
15. Rochoux MC, Emery C, Ricci S, Cuenot B, Trouvé A (2015) Towards predictive data-driven simulations of wildfire spread—part ii: ensemble Kalman filter for the state estimation of a front-tracking simulator of wildfire spread. *Nat Hazards Earth Syst Sci* 15(8):1721
16. Rios O, Pastor E, Valero M, Planas E (2016) Short-term fire front spread prediction using inverse modelling and airborne infrared images. *Int J Wildland Fire* 25(10):1033
17. Zhang C, Rochoux M, Tang W, Gollner M, Filippi JB, Trouvé A (2017) Evaluation of a data-driven wildland fire spread forecast model with spatially-distributed parameter estimation in simulations of the fireflux i field-scale experiment. *Fire Saf J* 91:758
18. Gu F, Hu X (2008) In 2008 winter simulation conference, pp 2852–2860. IEEE

19. Xue H, Gu F, Hu X (2012) Data assimilation using sequential monte carlo methods in wildfire spread simulation. *ACM Trans Model Comput Simul (TOMACS)* 22(4):23
20. Da Silva W, Rochoux M, Orlande H, Colaço M, Fudym O, El Hafi M, Cuenot B, Ricci S (2014) Application of particle filters to regional-scale wildfire spread. *High Temp High Press* 43:415
21. Bai F, Gu F, Hu X, Guo S (2016) Particle routing in distributed particle filters for large-scale spatial temporal systems. *IEEE Trans Parallel Distrib Syst* 27(2):481
22. Mandel J, Beezley JD, Kochanski AK, Kondratenko VY, Kim M (2012) Assimilation of perimeter data and coupling with fuel moisture in a wildland fire—atmosphere dddas. *Proc Comput Sci* 9:1100
23. Rochoux MC, Emery C, Ricci S, Cuenot B, Trouvé A (2014) Towards predictive simulation of wildfire spread at regional scale using ensemble-based data assimilation to correct the fire front position. *Fire Saf Sci* 11:1443
24. Safi Y, Bouroumi A (2013) Prediction of forest fires using artificial neural networks. *Appl Math Sci* 7(6):271
25. Castelli M, Vanneschi L, Popović A (2015) Predicting burned areas of forest fires: an artificial intelligence approach. *Fire Ecol* 11(1):106
26. Storer J, Green R (2016) PSO trained neural networks for predicting forest fire size: a comparison of implementation and performance. In: 2016 international joint conference on neural networks (IJCNN), pp 676–683
27. Naganathan H, Seshasayee SP, Kim J, Chong WK, Chou JS (2016) Wildfire predictions: determining reliable models using fused dataset. *Glob J Comput Sci Technol* 16(4):35–46
28. Cao Y, Wang M, Liu K (2017) Wildfire susceptibility assessment in southern china: a comparison of multiple methods. *Int J Disaster Risk Sci* 8(2):164
29. McCormick RJ, Brandner TA, Allen TF (2001) Toward a theory of meso-scale wildfire modeling: a complex systems approach using artificial neural networks. Ph.D. thesis, University of Wisconsin, Madison
30. McCormick RJ (2002) On developing a meso-theoretical viewpoint of complex systems by exploring the use of artificial neural networks in modeling wildfires. In: ForestSAT symposium, Edinburgh
31. LeCun Y, Boser B, Denker JS, Henderson D, Howard RE, Hubbard W, Jackel LD (1989) Backpropagation applied to handwritten zip code recognition. *Neural Comput* 1(4):541
32. Krizhevsky A, Sutskever I, Hinton GE (2012) Imagenet classification with deep convolutional neural networks. In: Pereira F, Burges CJC, Bottou L, Weinberger KQ (eds) *Advances in neural information processing systems 25: 26th annual conference on neural information processing systems 2012*, 3–6 December 2012. Lake Tahoe, NV, pp 1097–1105
33. Goodfellow I, Bengio Y, Courville A (2016) *Deep learning* (MIT Press). <http://www.deeplearningbook.org>. Accessed 27 Nov 2018
34. Kulkarni TD, Whitney WF, Kohli P, Tenenbaum J (2015) Deep convolutional inverse graphics network. In: Cortes C, Lawrence ND, Lee DD, Sugiyama M, Garnett R (eds) *Advances in neural information processing systems 28: annual conference on neural information processing systems 2015*, 7–12 December 2015. Montreal, QC, pp 2539–2547
35. Chen X, Duan Y, Houthoofd R, Schulman J, Sutskever I, Abbeel P (2016) Infogan: interpretable representation learning by information maximizing generative adversarial nets. In: Lee DD, Sugiyama M, Luxburg UV, Guyon I, Garnett R (eds) *Advances in*

- neural information processing systems 29: annual conference on neural information processing systems 2016, 5–10 December 2016. Barcelona, pp 2172–2180
36. Liu MY, Tuzel O (2016) Coupled generative adversarial networks. In: Lee DD, Sugiyama M, Luxburg UV, Guyon I, Garnett R (eds) *Advances in neural information processing systems 29: annual conference on neural information processing systems 2016*, 5–10 December 2016. Barcelona, pp 469–477
  37. Zhu JY, Park T, Isola P, Efros AA (2017) Unpaired image-to-image translation using cycle-consistent adversarial networks. In: *Proceedings of the IEEE international conference on computer vision*, pp 2223–2232
  38. Yi Z, Zhang H, Tan P, Gong M (2017) Dualgan: unsupervised dual learning for image-to-image translation. In: *Proceedings of the IEEE international conference on computer vision*, pp 2849–2857
  39. Albin FA (1976) Estimating wildfire behavior and effects. Technical report, USDA Forest Service
  40. Andrews PL (2012) Modeling wind adjustment factor and midflame wind speed for Rothelmer's surface fire spread model, General technical reports RMRS-GTR-266, vol 39. Department of Agriculture, Forest Service, Rocky Mountain Research Station, Fort Collins, CO, p 213
  41. Wagner CV (1969) A simple fire-growth model. *For Chron* 45(2):103
  42. Green D, Gill AM, Noble I (1983) Fire shapes and the adequacy of fire-spread models. *Ecol Model* 20(1):33
  43. Andrews PL (2009) Behaveplus fire modeling system, version 5.0: variables. General technical reports RMRS-GTR-213 revised, vol 111. Department of Agriculture, Forest Service, Rocky Mountain Research Station, Fort Collins, CO, p 213
  44. Nelson RM Jr (2002) An effective wind speed for models of fire spread. *Int J Wildland Fire* 11(2):153
  45. Rollins MG (2009) Landfire: a nationally consistent vegetation, wildland fire, and fuel assessment. *Int J Wildland Fire* 18(3):235
  46. Maas AL, Hannun AY, Ng AY (2013) Rectifier nonlinearities improve neural network acoustic models. *Proc ICML* 30:3
  47. He K, Zhang X, Ren S, Sun J (2015) Delving deep into rectifiers: surpassing human-level performance on imagenet classification. In: *Proceedings of the IEEE international conference on computer vision*, pp 1026–1034
  48. Abadi M, Agarwal A, Barham P, Brevdo E, Chen Z, Citro C, Corrado GS, Davis A, Dean J, Devin M, Ghemawat S, Goodfellow I, Harp A, Irving G, Isard M, Jia Y, Jozefowicz R, Kaiser L, Kudlur M, Levenberg J, Mané D, Monga R, Moore S, Murray D, Olah C, Schuster M, Shlens J, Steiner B, Sutskever I, Talwar K, Tucker P, Vanhoucke V, Vasudevan V, Viégas F, Vinyals O, Warden P, Wattenberg M, Wicke M, Yu Y, Zheng X (2015) TensorFlow: large-scale machine learning on heterogeneous systems. <https://www.tensorflow.org/>. Accessed 14 Apr 2018
  49. Filippi JB, Mallet V, Nader B (2014) Representation and evaluation of wildfire propagation simulations. *Int J Wildland Fire* 23(1):46
  50. Zhang C, Collin A, Moireau P, Trouvé A, Rochoux M (2019) Front shape similarity measure for data-driven simulations of wildland fire spread based on state estimation: application to the rxcadre field-scale experiment. *Proc Combust Inst* 37(3):4201
  51. Chan TF, Vese LA (2001) Active contours without edges. *IEEE Trans Image Process* 10(2):266